# Combined obliquity and precession pacing of the late Pleistocene glacial cycles

Peter Huybers

*Harvard University, Cambridge, MA*

**Milankovitch postulated that deglaciations occur when Earth's obliquity is high and precession brings Earth's eccentric orbit nearest the sun during northern summer, and this general concept has been elaborated to show how precession, obliquity, or combinations of both could govern the timing of deglaciations. Earlier observational tests indicate that obliquity paces the late Pleistocene glacial cycles, but are inconclusive with regard to precession because the shorter precession period demands greater time accuracy. Here, both obliquity and precession are shown to pace the timing of late Pleistocene glacial cycles. Requisite time control comes from a new tuning algorithm that calls on the orthogonality between precession and obliquity variations in order to avoid circularity and check for accuracy. A second test confirms combined orbital pacing without recourse to orbital tuning. Both tests support the Milankovitch hypothesis, but are also consistent with the duration of Southern Hemisphere summer pacing deglaciations.**

During the late Pleistocene—roughly over the last million years—Northern Hemisphere continental ice has alternately covered much of northern North America and Fennoscandia and then retreated to today's relatively ice-free conditions at approximately 100,000 year intervals. The cause of these massive shifts in climate remains unclear—less for lack of hypotheses, of which there are now over thirty, and more for lack of means to choose between them. Most of the models proposed over the last two centuries have called on the precession of the equinoxes relative to Earth's eccentric orbit[1–3], changes in Earth's obliquity[4,5], or some combination of both[6–11] to control the glacial cycles, though mechanisms wholly internal to the climate system have also been put forward[12,13]. Observational tests indicate that obliquity paces the $\sim$100 ky glacial cycles[5,14], helping narrow the list of viable mechanisms, but tests of precession's role have been inconclusive (i.e. $p > 0.05$) because of small sample sizes and uncertain timing[5,14,15]. A definitive test of precession only becomes possible if the timing of the majority of late Pleistocene glacial cycles can be determined to within a small fraction of precession's period.

## Testable tuning

A common means of estimating time in paleoclimate records is to stretch, squeeze, and shift a record's chronology in order to align it with a template indicative of changes in Earth's orbital and rotational configuration, a process generally referred to as orbital tuning[16,17]. The circularity that is otherwise inherent to orbital tuning and subsequent evaluation of orbital control can be avoided by calling upon the independence of obliquity and precession variability[18–20], which share less than 0.1% of their variance during the last million years. The strategy is to test for precession pacing using a chronology derived from tuning to obliquity, and vice-versa to test for obliquity pacing. Furthermore, the root-mean-square (rms) deviation between the

precession- and obliquity-tuned time estimates indicates the upper bound on the error associated with either tuned estimate. This follows from the expected value of rms($\delta_1 - \delta_2$) being greater than either rms($\delta_1$) or rms($\delta_2$), if $\delta_1$ and $\delta_2$ are independent random variables. Trials using synthetic records confirm that the obliquity- and precession-tuned time estimates are independent and indicate that results having an rms time difference of 5 ky or less are sufficiently accurate to test for precession pacing (Fig. S6). To highlight the internal test of time accuracy, this approach to orbital tuning is called TOTAL, for the Testable Orbital Tuning ALgorithm.

TOTAL is applied to a composite $\delta^{18}$O record whose initial timescale comes from sediment accumulation rates and radiometrically dated geomagnetic reversals[14]. The last million years are focused on because this epoch appears to have adequate obliquity and precession variability for the purposes of tuning. The average depth-derived time uncertainty during this interval is ±8 ky (1 s.d.), which is larger than estimated by (15), because along with sedimentation accumulation rate variability and other effects[14,21], the uncertainty in the $^{40}$K decay constant[22,23] is now accounted for, indicating that the age of the Matuyama-Brunhes geomagnetic reversal (M-B) is known only to within $780 \pm 8$ ky (1 s.d., see methods).

TOTAL has three steps. First, the time derivative of the $\delta^{18}$O record is taken in order to suppress the saw-tooth structure in late Pleistocene $\delta^{18}$O, increase the fraction of variance at the obliquity and precession bands, and provide a plausible physical relationship between orbital forcing and the climate's response[24]. Second, terminations are identified as instances when the rate-of-change of $\delta^{18}$O exceeds 0.095‰ per ky, a threshold chosen to yield terminations consistent with those identified by ref. 25, excepting that termination 3 inevitably has two components, labeled 3a and 3b (Fig. 1b). $\delta^{18}$O segments corresponding to each termination are defined to

extend to the abutting terminations (Fig. 1c). Finally, the lagged cross-correlation is computed between each $\delta^{18}$O segment and either the obliquity or precession variability[26], where the lag giving maximum cross-correlation indicates the time adjustment. The complete code and all data can be downloaded as supplemental information.

Application of TOTAL to the $\delta^{18}$O record yields an rms difference between obliquity- and precession-tuned estimates of 2.3 ky (Table 1), indicating sufficient accuracy to test for precession pacing. The probability of obtaining such a small rms deviation purely by chance is exceedingly small ($p < 0.001$). The only substantial discrepancy occurs for termination 5, for which the precession time estimate is 6 ky younger (Fig. 1d), but this time estimate is suspect anyway because the corresponding $\delta^{18}$O segment has the lowest cross-correlation with precession ($r = 0.19, p > 0.2$, Table S1) and corresponds to the interval with the lowest average eccentricity of any of the segments.

TOTAL's results can also be compared against independent radiometric dates. A compilation of 18 different Uranium-series constraints upon the timing of terminations 2 through 4 from corals, speleothems, and bulk sediments strongly supports the accuracy of TOTAL's results over those of the depth-derived times (Table 1, Fig. S9). The rms difference between TOTAL's results and the collection of radiometric dates is only 5 ky, where one radiometric estimate [27] for the age of termination 4 has been excluded because it is inconsistent with the others. Such a small rms indicates that the correct orbital cycles are identified, and is consistent with a 2.3 ky uncertainty in TOTAL's estimates, given an average 1.9 ky radiometric uncertainty (1 s.d.) and assuming a 4 ky uncertainty (1 s.d.) associated with aligning terminations in the $\delta^{18}$O record and radiometrically dated features (see the supplemental information).

The degree to which a system is finely tuned can be described by the electrical-engineer's Q value. The Q value—or quality value—is calculated as $f_o/\Delta f$ where $\Delta f$ is the frequency separation of a spectral peak at half its maximum power. Often used to measure resonance, the Q value is only used here to describe the sharpness of the spectral peak. The initial depth-derived timescale gives a Q value of 6.2 and 3.9 for the precession and obliquity peaks, respectively (Fig. 1e). Tuning to obliquity increases the Q value associated with precession to 7.9 and that associated with obliquity to 4.4 (Fig. 1f), and tuning to precession increases them to 7.4 and 4.4 (Fig. 1g), lending further support for the accuracy of the tuned results. Tuning does not, however, increase the Q value associated with the 100 ky peak, consistent with its being a paced oscillation[3,5,11,28], as opposed to a fundamental tone[29].

**Testing precession's role**

It is well established that the insolation variations associated with changes in the orientation of Earth's spin axis and orbital geometry influence Pleistocene climate[3], but the more specific question of whether the precession of the equinoxes controls the $\sim$100 ky glacial/interglacial cycles remains open. Precession alters diurnal average insolation intensity by 30 W/m$^2$ or more on a given day of the year, suggesting a powerful forcing, yet these anomalies are exactly counterbalanced across the seasons so that annual insolation at any latitude is independent of precession[30]. Furthermore, proxies of early Pleistocene glaciation show strong obliquity and little precession variability, indicating that precession had negligible influence during a recent epoch of glaciation[31]—though see ref. 32 for an alternate view. It is useful to empirically test precession's role in governing late Pleistocene glaciation.

Precession pacing of glacial cycles is assessed by quantifying the stability of precession's phase across late Pleistocene glacial terminations, where phase stability is measured using Rayleigh's $R$ (see methods). The significance of the sampled $R$ value is assessed within the context of a null hypotheses, $H_0$, that termination timing is independent of phase, and an alternate hypothesis, $H_1$, that terminations cluster near a particular phase of precession. Numerous models were explored for estimating the distribution of $H_0$, including some that account for the previously identified obliquity pacing of deglaciations[5,14] (Fig. S11), but the model found to give the most stringent test—yielding the highest critical values—comes from a modified random walk representing ice-volume variability[5],

$$v_t = v_{t-1} + \eta_t, \text{ and if } v_t \geq h_t, \text{ terminate.} \quad (1)$$

Ice volume ($v$) accumulates by a random increment ($\eta_t$) during each 1-ky time step, until a threshold ($h$) is surpassed, and the termination of all ice is prescribed at a rate of -10 units per ky. Defining $h_t = 90$, and drawing $\eta_t$ from a normal distribution with unit mean and two units of standard deviation gives glacial cycles of $100 \pm 20$ ky, consistent with observations[5]. Rayleigh's $R$ is then computed from precession phases across 11 model terminations, and the distribution of $R$ estimated from $10^5$ model runs. $H_1$ is similarly derived from Eq. 1, but after modifying the threshold condition to be sensitive to the amount of insolation received during the summer, $h_t = 100 - J_t$. $J_t$ is the summer energy[31] calculated at 65°N for insolation intensities exceeding 340 W/m$^2$, which gives approximately equal precession- and obliquity-period variability[33], and it is scaled to have zero mean and a variance of (24 units)$^2$, where the rationale for this specific parametrization is given later. Under $H_1$, terminations tend to trigger as ice volume grows, obliquity increases, and precession brings Earth's eccentric orbit nearer

the sun during Northern Hemisphere summer. The influence of timescale errors upon $H_1$ are accounted for by perturbing termination ages by ±8 ky (1 s.d.) for the depth-derived times and by ±2.3 ky for the TOTAL times.

The power of the precession test—i.e. the probability of rejecting $H_0$ at 95% confidence when $H_1$ is correct—increases from 0.05 to 0.57 after tuning to obliquity because of the reduction in time uncertainty, suggesting that a skillful precession test is now possible (Fig. 2e). Furthermore, the precession $R$ value increases from 0.16 ($p = 0.77$) to 0.65 ($p = 0.01$), consistent with $H_1$ and permitting confident rejection of $H_0$ (Fig. 2b,e). The most discordant precession phases occur for terminations 5, 6, and 9, when eccentricity is anomalously small. If the $R$ value is recalculated weighting each precession phase according to the eccentricity at each termination (see methods), the power of the test increases to 0.69 and the $R$ value increases to 0.81 ($p = 0.001$, Fig. 2c,f). Precession thus paces late-Pleistocene deglaciations, especially when eccentricity is large. A similar treatment is possible for obliquity, and tuning exclusively to precession increases the power of the (unweighted) obliquity test from 0.29 to 0.96 and the $R$ value from 0.50 ($p = 0.05$) to 0.69 ($p = 0.003$), reinforcing earlier findings that obliquity also paces deglaciations[5,14] (Fig. 2a,d).

To assess robustness, TOTAL is also applied to rescaled versions of the depth-derived times consistent with M-B ages ranging over 780±16 ky (2 s.d.). Precession test results are unaffected because obliquity tuning invariably realizes similar ages. Obliquity test results are more sensitive because they depend upon tuning to shorter-period precession variations, but every realization that is insignificant has an rms deviation between the orbitally-derived times that exceeds 5 ky, indicating that those timescales are implausible and should be ignored (Fig. S10).

Note, also, that there appears no reason to expect to have obtained the foregoing, highly significant results if the timescale is substantially in error.

**Combined obliquity and precession pacing**

The Rayleigh's $R$ results indicate that deglaciations tend to occur when obliquity and precession are near maxima (Fig. 2a-c). By implication, the time difference between a given precession maximum and the nearest obliquity maximum tends to be smaller during terminations. Indeed, when the obliquity-tuned timescale is used to match precession maxima and terminations, the dispersion of time differences between precession and obliquity maxima during terminations is markedly smaller (16 ky$^2$) than the dispersion away from terminations (34 ky$^2$, $p < 0.001$, $n = 12$, see Fig. 2g and methods). These results are also robust to timing errors, requiring only that the correct precession maximum tends to be identified with each termination, and similar results are obtained using the precession-tuned ($p < 0.001$, $n = 12$) and, moreover, the raw depth-derived timescale ($p = 0.002$, $n = 12$). Depth-derived timescale results remain significant ($p \leq 0.05$) until $\pm 8$ ky (1 s.d.) or greater perturbations to the M-B age lead to the identification of substantially different precession maxima.

Both the Rayleigh's $R$ and dispersion tests provide extremely strong evidence for obliquity and precession pacing of late Pleistocene glacial cycles. Taking these test results together, it appears safe to discard those models of late Pleistocene glacial cycles that are incapable of explaining combined obliquity- and precession-pacing.

In addition to the orbital configuration, it has also been suggested that growth of ice vol-

ume promotes destabilization and deglaciation[7,28]. One can further question whether stronger orbital forcing will trigger a deglaciation at smaller amounts of ice volume? The maximum $\delta^{18}$O found just prior to each late-Pleistocene deglaciation roughly indicates the amount of accumulated ice, and it has a cross-correlation of -0.55 ($p = 0.04, n = 11$) with the value of eccentricity at each termination. Apparently, the climate is nudged out of glaciation sooner when eccentricity—and, therefore, the amplitude of precession forcing—is large. Because interglacial values of $\delta^{18}$O are less variable than glacial values, this relationship also implies that the amplitude of the $\sim$100 ky glacial cycles are smaller when eccentricity is large, consistent with the recent findings reported in ref. 34.

The foregoing statistical results can be succinctly illustrated by replacing the stochastic variable in Eq. 1 with its mean value. A simulated annealing algorithm then indicates that the highest cross-correlation between $v(t)$ and the negative of the $\delta^{18}$O record occurs for the parametrizations used earlier in estimating $H_1$, regardless of whether the obliquity ($r = 0.79$) or precession-tuned timescale ($r = 0.75$) is used. Such correlations are very high relative to other simple model fits, particularly given the small number of adjustable parameters[35] (Fig. 3a). This version of Eq. 1 reproduces the basic sawtooth structure of late-Pleistocene glacial cycles over the last million years in terms of timing and amplitude, and illustrates how obliquity, precession, and the growth of ice volume can combine to set the timing and amplitude of the late-Pleistocene glacial cycles.

## Discussion and conclusions

Elsewhere[15], it was found that the timing of the last four terminations recorded in the

Dome Fuji deuterium record led to higher $R$ values for precession (0.82, p=0.06) than for obliquity (0.70, p=0.15). TOTAL's results also give higher precession ($0.91$, $p = 0.02$) than obliquity $R$ values ($0.61$, $p = 0.24$) when only the last four terminations are considered, but this situation is reversed if seven or more terminations are considered (Fig. S13). Although this hints at stronger precession control more recently, this situation could also arise from random statistical fluctuations, and one cannot distinguish whether obliquity or precession exercise greater influence—both pace the timing of terminations in the sense of refs. 3 and 11 but neither exercise exclusive control.

Combined orbital pacing is consistent with earlier findings that the intervals between successive deglaciations cluster into 80 or 120 ky periods[5,14], indicative of two or three obliquity cycles. Precession, with its $\sim$20 ky period, achieves a maximum during nearly every interval of above average obliquity, given its $\sim$40 ky period, but the reverse does not hold (e.g. Fig. 1a). Therefore, precession will tend to influence the precise timing of a deglaciation within an obliquity cycle, but obliquity will more fundamentally govern the interval between deglaciations. Its rather like the minute and hour hands of a clock, where the longer-period cycle of the hour hand determines the interval between successive 12 o'clocks. Whether precession also influences the precise timing of terminations during the early Pleistocene, when deglaciations occur more nearly every 40 ky, remains an open question[31,32]. Perhaps terminations then occurred nearly every time above average obliquity and precession maxima coincide, as can be obtained from setting the threshold in Eq. 1 to lower values.

Icesheets tend to collapse under orbital conditions of high obliquity, alignment of perihelion with Northern Hemisphere summer solstice, and large eccentricity, at least during the

late Pleistocene. During these terminations, summer insolation averages 30 $W/m^2$ greater at high northern latitudes (Fig. 3b), consistent with Milankovitch's hypothesis[6] and elaborations thereof[7–9,11]. However, other aspects of this orbital configuration may also influence deglaciation. For example, when perihelion is aligned with Northern Hemisphere summer solstice, aphelion aligns to increase the duration of Southern Hemisphere summer (Fig. 3b), and this may increase the evasion of $CO_2$ out of the Southern Ocean and into the atmosphere[36–39]. The climate system is thoroughly interconnected across temporal and spatial scales, and just as obliquity and precession do not act in isolation, no one region should be expected to exert exclusive influence upon deglaciation.

**Methods Summary**

When applying TOTAL, the cross-correlation between orbital variability and each segment of the $\delta^{18}$O record centered on a termination is computed over $\pm$20 ky for obliquity and $\pm$8 ky for precession. Tuned timescales are then obtained by linearly interpolating the original depth-derived timescale between the termination times that maximize correlation. The initial depth-derived times are rescaled according to $\delta t$ perturbations of the Matuyama-Brunhes age by multiplying by $(780\text{ky} + \delta t)/780\text{ky}$.

Rayleigh's $R$[5,40] is computed as $\frac{1}{\sum w_n}\left|\sum_{n=1}^{N} w_n \left(\cos\phi_n + i\sin\phi_n\right)\right|$, where $\phi_n$ is the phase of either obliquity or precession stroboscopically sampled at the $n$th glacial termination and $w_n$ weights each phase. Brackets indicate the magnitude, making $R$ real and non-negative. Each termination is counted as a degree of freedom for the phase, except terminations 3a and 3b, which are together counted as one.

The distribution of $H_0$ is estimated by initializing Eq. 1 at $t = -1500$ ky with a random ice volume uniformly distributed between 0 and $h = 90$ units, and R-values are realized from the orbital phases associated with the 11 youngest terminations in each of $10^5$ model realizations. $H_0$ can be rejected at 95% confidence at $R = 0.51$ (obliquity) and $R = 0.52$ (precession) and at 99% confidence at $R = 0.62$ (obliquity) and $R = 0.63$ (precession), given constant $w_n$. Eccentricity weighting increases the 95% and 99% confidence levels for precession to 0.56 and 0.67. $H_1$ is similarly estimated from Eq. 1, but using a threshold that depends on summer energy[31], which is calculated as the sum of insolation at 65°N on days having an average insolation exceeding 340 W/$m^2$.

Differences in the temporal dispersion between obliquity and precession maxima are tested for using a one-sided Ansari-Bradley test, which does not require an assumption of normality. Also, temporal differences are consistent with a median of zero, as is expected and is required for this test. 12 degrees of freedom are used because terminations 3a and 3b are associated with distinct precession cycles.

## Bibliography


1. Adhémar, J. A. *Révolutions de la Mer: Déluges Períodiques* (Carilian-Goeury et V. Dalmont, Paris, Paris, 1842).

2. Croll, J. *Climate and Time* (Appleton and Co., 1875).

3. Hays, J., Imbrie, J. & Shackleton, N. Variations in the Earth's orbit: Pacemaker of the ice ages. *Science* **194**, 1121–1132 (1976).

4. Liu, H. Phase modulation effect of the Rubincam insolation variations. *Theor. Appl. Climatol.* **61**, 217–229 (1998).

5. Huybers, P. & Wunsch, C. Obliquity pacing of the late Pleistocene glacial terminations. *Nature* **434**, 491–494 (2005).

6. Milankovitch, M. *Kanon der Erdbestrahlung und seine Andwendung auf das Eiszeitenproblem* (Royal Serbian Academy, Belgrade, 1941).

7. Imbrie, J. & Imbrie, J. Modeling the climatic response to orbital variations. *Science* **207**, 943–953 (1980).

8. Paillard, D. The timing of Pleistocene glaciations from a simple multiple-state climate model. *Nature* **391**, 378–391 (1998).

9. Berger, A., Li, X. & Loutre, M. Modelling northern hemisphere ice volume over the last 3Ma. *Quaternary Science Reviews* **18**, 1–11 (1999).

10. Saltzman, B. *Dynamical Paleoclimatology: Generalized Theory of Global Climate Change* (Academic Press, San Diego, 2002).

11. Tziperman, E., Raymo, M., Huybers, P. & Wunsch, C. Consequences of pacing the Pleistocene 100 kyr ice ages by nonlinear phase locking to Milankovitch forcing. *Paleoceanography* **21**, PA4206 (2006).

12. Ghil, M. Cryothermodynamics: the chaotic dynamics of paleoclimate. *Physica D* **77**, 130–159 (1994).

13. Wunsch, C. The spectral description of climate change including the 100ky energy. *Climate Dynamics* **20**, 353–363 (2003).

14. Huybers, P. Glacial variability over the last two million years: an extended depth-derived agemodel, continuous obliquity pacing, and the Pleistocene progression. *Quat. Sci. Rev.* **26**, 37–55 (2007).

15. Kawamura, K. *et al.* Northern Hemisphere forcing of climatic cycles in Antarctica over the past 360,000 years. *Nature* **448**, 912–916 (2007).

16. Imbrie, J. *et al.* The orbital theory of Pleistocene climate: Support from a revised chronology of the marine delta-18o record. In Berger, A. e. a. (ed.) *Milankovitch and Climate, Part 1*, 269–305 (D. Riedel Publishing Company, 1984).

17. Lisiecki, L. & Lisiecki, P. Application of dynamic programming to the correlation of paleoclimate records. *Paleoceanography* **17**, 1–1,1–12 (2002).

18. Kominz, M., Heath, G., Ku, T. & Pisias, N. Brunhes time scales and the interpretation of climatic change. *Earth and Planetary Science Letters* **45**, 394–410 (1979).

19. Muller, R. & MacDonald, G. *Ice Ages and Astronomical Causes* (Springer, 2000).

20. Karner, D., Levine, J., Medeiros, B. & Muller, R. Constructing a stacked benthic $\delta^{18}$O record. *Paleoceanography* (2002).

21. Huybers, P. & Wunsch, C. A depth-derived Pleistocene age-model: Uncertainty estimates, sedimentation variability, and nonlinear climate change. *Paleoceanography* **19**, 10.1029/2002PA000857 (2004).

22. Min, K., Mundil, R., Renne, P. & Ludwig, K. A test for systematic errors in 40Ar/39Ar geochronology through comparison with U/Pb analysis of a 1.1-Ga rhyolite. *Geochimica et Cosmochimica Acta* **64**, 73–98 (2000).

23. Kuiper, K. *et al.* Synchronizing rock clocks of Earth history. *Science* **320**, 500 (2008).

24. Roe, G. In defense of Milankovitch. *Geophysical Research Letters* **33** (2006).

25. Broecker, W. Terminations. In Berger, A. e. (ed.) *Milankovitch and climate, Part2*, 687–698 (D. Riedel, Hingham, 1984).

26. Laskar, J. *et al.* A long-term numerical solution for the insolation quantities of the Earth. *Astronomy and Astrophysics* **428**, 261–285 (2004).

27. Henderson, G., Robinson, L., Cox, K. & Thomas, A. Recognition of non-Milankovitch sea-level highstands at 185 and 343 thousand years ago from U-Th dating of Bahamas sediment. *Quaternary Science Reviews* **25**, 3346–3358 (2006).

28. Raymo, M. E. The timing of major climate terminations. *Paleoceanography* **12**, 577–585 (1997).

29. Muller, R. & MacDonald, G. Glacial cycles and astronomical forcing. *Science* **277**, 215 (1997).

30. Herschel, J. On the Astronomical Causes which may influence Geological Phenomena. *Transactions of the Geological Society of London* **3**, 293–300 (1832).

31. Huybers, P. Early Pleistocene glacial cycles and the integrated summer insolation forcing. *Science* **313**, 508–511 (2006).

32. Raymo, M., Lisiecki, L. & Nisancioglu, K. Plio-Pleistocene ice volume, Antarctic climate, and the global $\delta^{18}$O record. *Science* **313**, 10.1126/science.1123296 (2006).

33. Huybers, P. & Tziperman, E. Integrated summer insolation forcing and 40,000 year glacial cycles: The perspective from an ice-sheet/energy-balance model. *Paleoceanography* **23** (2008).

34. Lisiecki, L. Links between eccentricity forcing and the 100,000-year glacial cycle. *Nature Geoscience* **3**, 349–352 (2010).

35. Roe, G. & Allen, M. A comparison of competing explanations for the 100,000-yr ice age cycle. *Geophysical Research Letters* **26**, 2259–2262 (1999).

36. Broecker, W. & Henderson, G. The sequence of events surrounding Termination II and their implications for the cause of glacial-interglacial $CO_2$ changes. *Paleoceanography* **13**, 352–364 (1998).

37. Schulz, K. & Zeebe, R. Pleistocene glacial terminations triggered by synchronous changes in Southern and Northern Hemisphere insolation: The insolation canon hypothesis. *Earth and Planetary Science Letters* **249**, 326–336 (2006).

38. Huybers, P. & Denton, G. Antarctic temperature at orbital time scales controlled by local summer duration. *Nature Geoscience* **1**, 787–792 (2008).

39. Timmermann, A., Timm, O., Stott, L. & Menviel, L. The roles of CO2 and orbital forcing in driving Southern Hemispheric temperature variations during the last 21,000 years. *J. of Climate* (2009).

40. Mardia, K. Statistics of directional data. *Journal of the Royal Statistical Society. Series B (Methodological)* **37**, 349–393 (1975).

41. Joussaume, S. & Braconnot, P. Sensitivity of paleoclimate simulation results to season definitions. *Journal of Geophysical Research* **102**, 1943–1956 (1997).

**Supplemental Information** is linked to the online version of the paper at www.nature.com/nature.

**Acknowledgments** This work benefited from comments by Geoffrey Gebbie, Lorraine Lisiecki, Alexander Stine, Carl Wunsch, and two anonymous reviewers.

**Author Information** The author declares no competing financial interests. Correspondence and requests for materials should be addressed to phuybers@fas.harvard.edu.

Figure 1: Tuning the late Pleistocene $\delta^{18}$O record. **(a)** Obliquity (red) and precession (gold) variability over the last million years[26]. **(b)** Rate-of-change of $\delta^{18}$O in ‰/ky from the composite record of (10). The horizontal dashed line indicates the threshold above which a termination is defined to occur, and the vertical solid lines indicate the point having the maximum rate of change during each termination. **(c)** The lagged cross-correlation between segments encompassing each termination and obliquity (red, $\pm$20 ky lags) or precession (gold, $\pm$8 ky lags). Colored horizontal bars indicate the time adjustments needed to maximize correlation. **(d)** The lags resulting in the maximum cross-correlation for obliquity versus that for precession, with numbers indicating terminations. **(e)** A power-spectral estimate of the rate-of-change of $\delta^{18}$O plotted on linear axes. Peaks are at the 1/100 ky$^{-1}$, 1/41 ky$^{-1}$ (obliquity), and 1/22 ky$^{-1}$ (precession) bands, and the Q value and half widths are indicated for the latter two. Subsequent panels are similar to (e) but after tuning **(f)** to obliquity and **(g)** to precession.

Figure 2: Testing the orbital hypothesis. **(a)** The phase of obliquity during each termination (indicated by the numbers) is shown for the untuned (black squares) and precession tuned (red circles) timescales with the 12 o'clock position indicating maximum obliquity. Spokes indicate the vector average of each set of phase estimates, where the vector's magnitude equals Rayleigh's $R$, and the gray shaded disk indicates the 95% confidence level. Clustering of the obliquity phases is significant using either timescale. **(b)** Similar to (a) but for precession, showing phases from the untuned (black) and obliquity-tuned timescales (red). **(c)** Modification of (b) having precession vectors whose magnitude is proportional to eccentricity (dashed lines) and the vector average (solid line). Tuning to obliquity and weighting by eccentricity both greatly increases the significance of precession pacing. **(d)** The estimated null ($H_0$, dashed) and alternate ($H_1$, solid) probability densities for obliquity pacing prior to tuning (black) and after tuning to precession (red), as well as the sample R-values prior to (black bar) and after tuning (red bar). **(e)** Similar to (d) but for the precession test before and after tuning to obliquity, and then **(f)** with eccentricity weighting. **(g)** The time of each precession maximum plotted against the temporal separation between that time and the nearest obliquity maximum. Circles indicate precession maxima associated with terminations according the obliquity-tuned timescale (red), as well as the single change when using the precession-tuned (green) or depth-derived times (blue).

Figure 3: Insolation pacing of glacial cycles. **(a)** Deterministic results from the simple glacial model (Eq. 1) after adjusting the summer energy threshold condition (gray line, scaled to normalized ice volume units) to maximize cross-correlation with the obliquity-tuned $\delta^{18}$O record (red line, also scaled to ice volume units). With some exceptions, both the timing and amplitude of the glacial cycles are reproduced. **(b)** The average insolation anomaly (W/m$^2$) during terminations. Anomalies are computed as the average insolation during both the obliquity and precession-estimated termination times relative to the average insolation over the last million years. Note that anomalies are shown relative to day of the year and not solar longitude[41].

| termination | 1 | 2 | 3a | 3b | 4 | 5 | 6 | 7 | 8 | 9 | 10 | 11 |
|---|---|---|---|---|---|---|---|---|---|---|---|---|
| depth-derived | 11 | 124 | 208 | 231 | 326 | 423 | 538 | 622 | 714 | 794 | 864 | 957 |
| precession-tuned | 13 | 127 | 216 | 239 | 334 | 415 | 536 | 621 | 713 | 793 | 864 | 958 |
| obliquity-tuned | 12 | 125 | 217 | 240 | 336 | 421 | 535 | 621 | 711 | 791 | 863 | 955 |
| young radiometric bound | | 123 | 217 | 235 | 328 | | | | | | | |
| old radiometric bound | | 137 | 226 | 255 | 338 | | | | | | | |

Table 1: Time estimates for each termination (ky ago). See the supplemental information for more on the radiometric bounds.

## Methods

**Testable Orbital Tuning ALgorithm:** TOTAL is applied to the time rate of change of a composite $\delta^{18}$O record[14]. Time control points (TCPs) are assigned at each termination, defined as maxima in the rate of decrease in $\delta^{18}$O, so long as those maxima exceed -0.095‰/ky. The initial time estimate depends on average accumulation rates and radiometric dates. Segments are then defined that are centered on one TCP and extend to the neighboring TCPs. The segments used for terminations 3a and 3b both extend to terminations 2 and 4. The lag at which maximum correlation occurs with obliquity or precession[26] is computed for each segment, yielding two independent tuning estimates. Maximum correlation is searched over plus or minus half the period associated with each orbital parameter: $\pm$20 ky for obliquity and $\pm$8 ky for precession. Some precession cycles are very short, $<$ 17 ky, and using the shorter period guards against obtaining multiple maxima in the lagged cross-correlation. Note that obliquity-tuned times suggest that precession-tuning underestimates the age adjustment required for terminations 3a, 3b, and 4, but by no more than a few ky (Table 1).

The root-mean-square difference between the original depth-derived times and either the precession- or obliquity-derived estimates is 5 ky, somewhat smaller than the estimated 8 ky rms uncertainty in the depth-derived times[14]. The adjustments show the autocorrelation expected from the cumulative nature of the time model errors[21], with terminations 2 through 4 adjusted toward older times and terminations 5 through 9 adjusted toward younger times (Figs. 1c,d). Successive termination time adjustments are partly dependent because of overlapping segments, but if segments are multiplied by a Hanning window to focus their variance on the central TCP, negligible changes in timing occur and the same test results are obtained, so this additional complication is not included. Tuned timescales are obtained by linearly interpolating the depth-derived times between the adjusted TCPs. See the supplemental information for more on the development of TOTAL, its performance when applied to synthetic records, and comparison

of its results against other time estimates.

**Matuyama-Brunhes age:** The age of marine isotopic stage 19.1 was earlier assumed to be constrained to $780 \pm 3$ ky (1 s.d.) by radiometric dating of the Matuyama-Brunhes geomagnetic reversal [14], but accounting for uncertainty in the $^{40}$K decay constant[22,23] indicates that $780 \pm 8$ ky (1 s.d.) is a better representation of the age uncertainty of both the M-B and stage 19.1 (see supplemental information). Depth-derived timescale uncertainty over the last million years is obtained by running a stochastic sediment accumulation rate model[14,21] with this more uncertain radiometric bound. Also, depth-derived times are rescaled to $\delta t$ perturbations of the M-B age by multiplying time by $(780\text{ky} + \delta t)/780\text{ky}$.

**Rayleigh's R** is used to asses the stability of the phase relationship between the timing of terminations and orbital variations, $R = \frac{1}{\sum w_n} \left| \sum_{n=1}^{N} w_n \left( \cos \phi_n + i \sin \phi_n \right) \right|$. Here, $\phi_n$ is the phase of either obliquity or precession stroboscopically sampled at the $n$th glacial termination. Brackets indicate the magnitude, making $R$ real and non-negative, with a maximum value of one when the phases are all equal. The phase of each orbital parameter, $\phi_n$, is computed by linearly interpolating a 360° change in phase with the elapsed time between successive maxima. Each termination is counted as a degree of freedom for the phase, except terminations 3a and 3b, which are together counted as one. The standard form of Rayleigh's $R$ has $w_n = 1$, but when samples are individually weighted, the form of the $R$ statistic closely resembles that for spectral coherence. Although TOTAL implicitly assumes a 90° phase shift between the forcing and response, given the use of the time-derivative of the $\delta^{18}$O record, this phase assumption does not influence Rayleigh's $R$ because it is insensitive to changes in the mean phase.

**Null and alternate hypotheses:** In order to derive a null distribution, Eq. 1 is initialized at $t = -1500$ ky with a random ice volume uniformly distributed between 0 and $h = 90$ units, and R-values are realized from the orbital phases associated with the 11 youngest terminations in each of $10^5$

model realizations. Given constant $w_n$, $H_0$ can be rejected at 95% confidence at $R = 0.51$ (obliquity) and $R = 0.52$ (precession), and at 99% confidence at $R = 0.62$ (obliquity) and $R = 0.63$ (precession). Eccentricity weighting reduces the degrees of freedom somewhat and increases the 95% and 99% confidence levels to 0.56 and 0.67. Eq. 1 could be made to account for previously identified obliquity pacing of deglaciations[5,14], but this would make $H_0$ substantially easier to reject (Fig. S12). Surrogate data techniques and other models were also explored, but also give a more easily rejected $H_0$ and, therefore, are not used. The alternate distribution is derived in a manner similar to the null, but with a time-variable threshold that depends on summer energy, $h_t = 100 - J_t$. $J$ is calculated as the sum of insolation at 65°N on days having an average insolation exceeding 340 W/m$^2$.

**Ansari-Bradley dispersion test:** The distribution of time between precession maxima and the nearest obliquity maximum is bounded at plus or minus half an obliquity cycle and, therefore, cannot be normal. Thus, instead of the the more common F-test, differences in dispersion are tested for using the Ansari-Bradley test, which does not require the assumption of a normal distribution. Temporal differences between precession and obliquity maixma are consistent with a zero median, as is expected for the observations and required for the test. Twelve degrees of freedom are used in computing significances because terminations 3a and 3b are associated with distinct precession cycles.

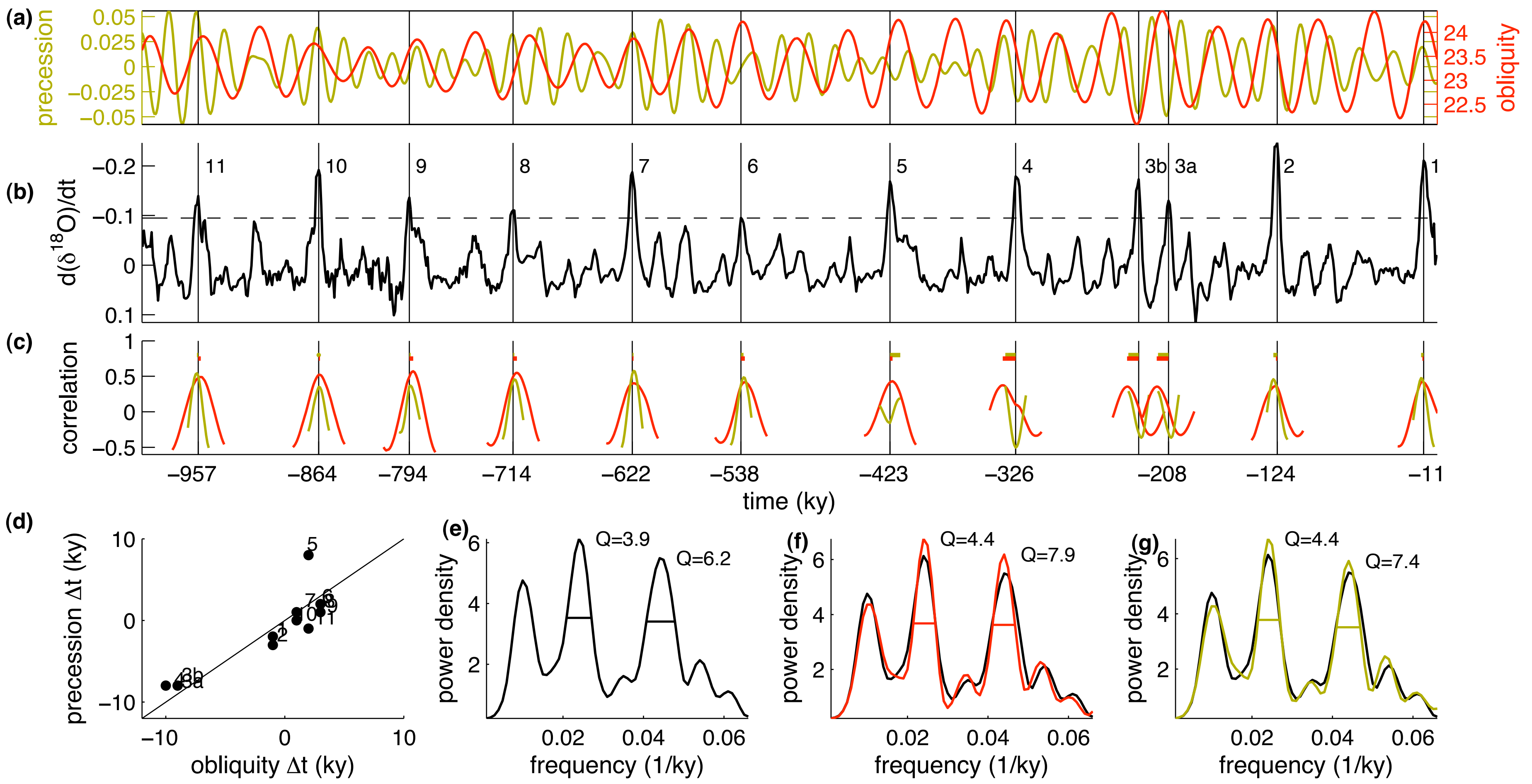

(a)
precession
obliquity
0.05
0.025
0
−0.025
−0.05
24
23.5
23
22.5
(b)
d(δ18O)/dt
−0.2
−0.1
0
0.1
11
10
9
8
7
6
5
4
3b
3a
2
1
(c)
correlation
1
0.5
0
−0.5
−957
−864
−794
−714
−622
−538
−423
−326
−208
−124
−11
time (ky)
(d)
precession Δt (ky)
obliquity Δt (ky)
10
0
−10
(e)
Q=3.9
Q=6.2
power density
frequency (1/ky)
(f)
Q=4.4
Q=7.9
(g)
Q=4.4
Q=7.4
0.02
0.04
0.06

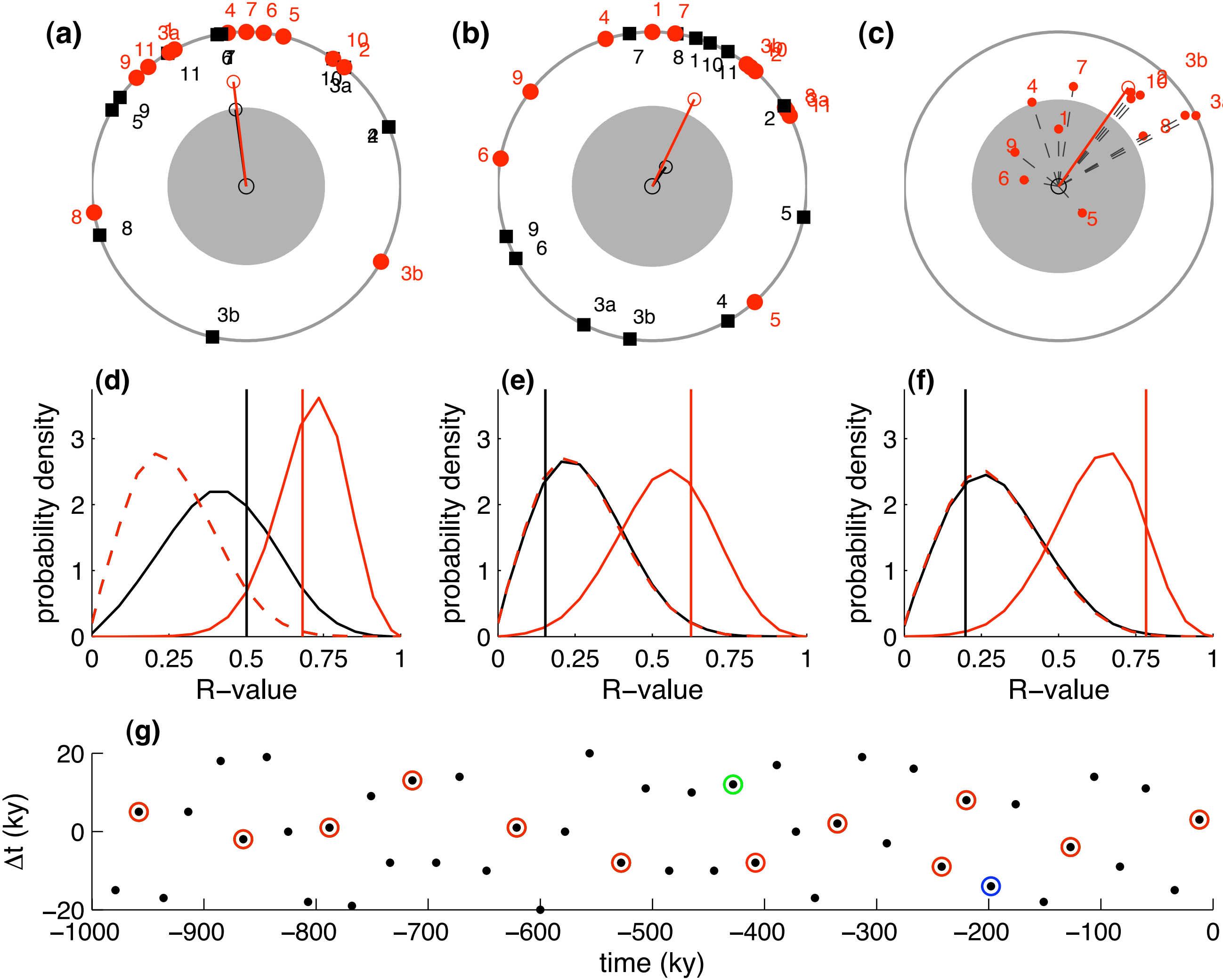

(a)
(b)
(c)
(d)
(e)
(f)
(g)
probability density
R−value
Δt (ky)
time (ky)

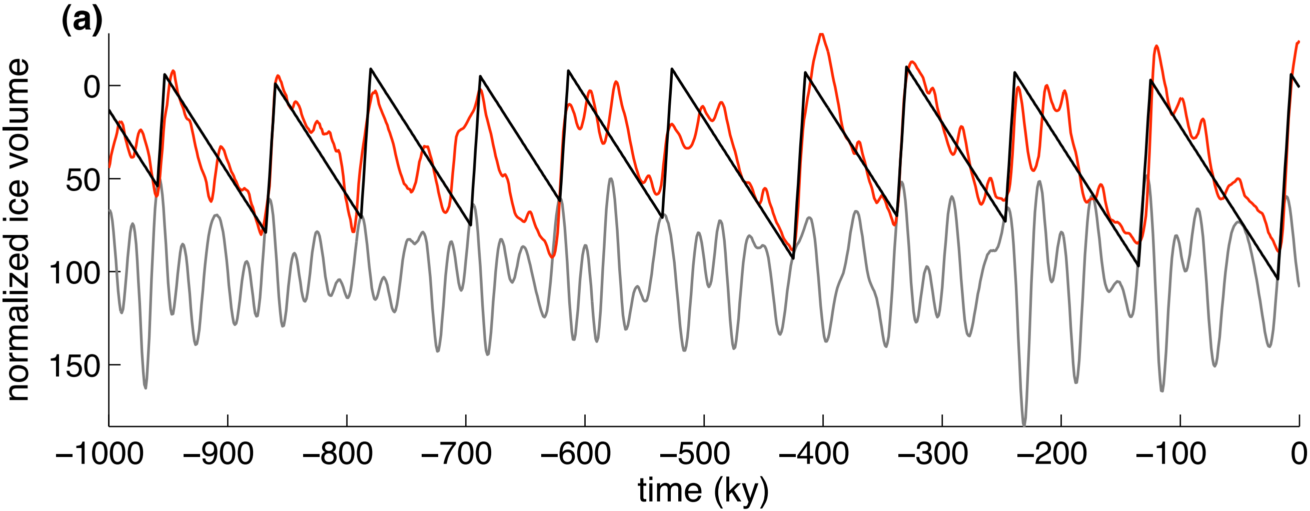

(a)
normalized ice volume
0
50
100
150
−1000
−900
−800
−700
−600
−500
−400
−300
−200
−100
0
time (ky)


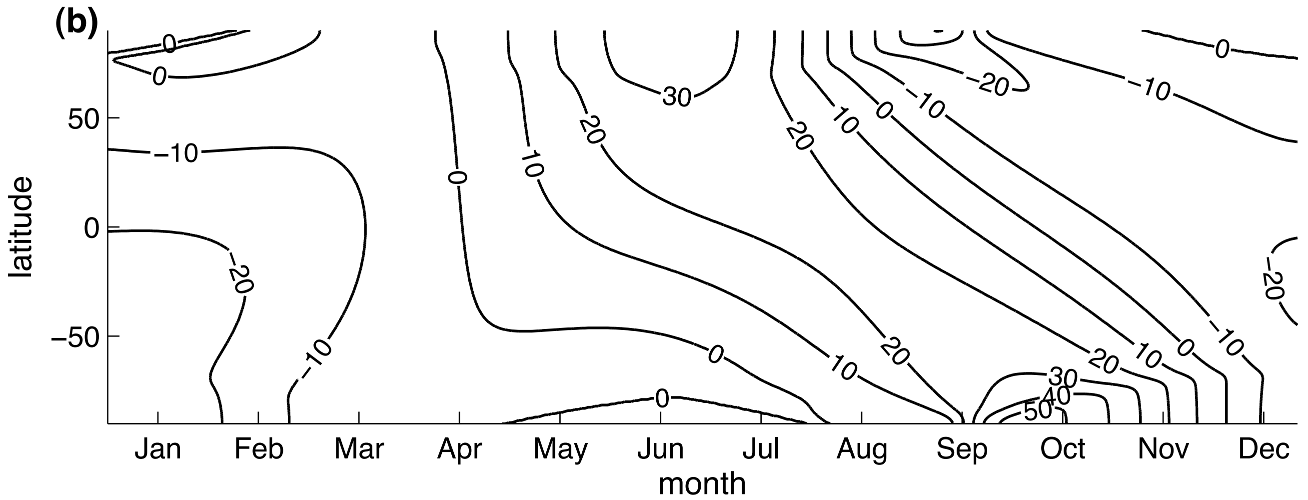

(b)
latitude
50
0
−50
Jan
Feb
Mar
Apr
May
Jun
Jul
Aug
Sep
Oct
Nov
Dec
month
0
−10
−20
10
20
30
40
50